Applied Surface Science xxx (2010) xxx–xxx

Contents lists available at ScienceDirect

Applied Surface Science

journal homepage: www.elsevier.com/locate/apsusc

Electrical and optical properties of thermally-evaporated thin films from $A_2[TiO(C_2O_4)_2]$ (A = K, PPh_4) and 1,8-dihydroxyanthraquinone

E. Carbia-Ruelas [a], M.E. Sánchez-Vergara [a,*], V. García-Montalvo [b], O.G. Morales-Saavedra [c], J.R. Álvarez-Bada [a]

[a] Coordinación de Ingeniería Mecatrónica. Facultad de Ingeniería, Universidad Anáhuac México Norte. Avenida Universidad Anáhuac 46, Col. Lomas Anáhuac, 52786, Huixquilucan, Estado de México, Mexico
[b] Instituto de Química, Universidad Nacional Autónoma de México. Circuito Exterior, Ciudad Universitaria, 04510, México, D. F, Mexico
[c] Centro de Ciencias Aplicadas y Desarrollo Tecnológico, Universidad Nacional Autónoma de México, CCADET-UNAM. A. P. 70-186, Coyoacán, 04510, México, D. F, Mexico

ARTICLE INFO

Article history:
Received 8 July 2010
Received in revised form 1 November 2010
Accepted 1 November 2010
Available online xxx

Dedicated to Professor Raymundo Cea Olivares on the occasion of his 60th birthday.

Keywords:
Thin films
Optical properties
Electrical properties
NLO-effect

ABSTRACT

In this work, the synthesis of molecular materials formed from $A_2[TiO(C_2O_4)_2]$ (A = K, PPh4) and 1,8 dihydroxyanthraquinone is reported. The synthesized materials were characterized by atomic force microscopy (AFM), infrared (IR) and ultraviolet-visible (UV–vis) spectroscopy. IR spectroscopy showed that the molecular-material thin-films, deposited by vacuum thermal evaporation, exhibit the same intramolecular vibration modes as the starting powders, which suggests that the thermal evaporation process does not alter the initial chemical structures. Electrical transport properties were studied by dc conductivity measurements. The electrical activation energies of the complexes, which were in the range of 0.003–1.16 eV, were calculated from Arrhenius plots. Optical absorption studies in the wavelength range of 190–1090 nm at room temperature showed that the optical band gaps of the thin films were around 1.9–2.3 eV for direct transitions Eg_d. The cubic NLO effects were substantially enhanced for materials synthesized from $K_2[TiO(C_2O_4)_2]$, where $\chi^{(3)}$ $(-3\omega; \omega, \omega, \omega)$ values in the promising range of 10^{-12} esu have been evaluated.

1. Introduction

Molecular materials have received an increasing interest due to their characteristic electrical properties, which may lead to semiconducting, conducting or insulating behavior [1–3]. These materials are formed from the organization and condensation of molecular units that may be organic and metalorganic species. Their microstructure is of particular interest, as they are generally formed by molecules displaying preferential paths for conductivity [4,5]. The molecules chosen as building blocks to make a conducting solid must lead to a packing that prioritizes the overlap of π-type orbitals in order to generate appropriate energy bands for the mobility of the charge carriers, and they must also be capable of giving or accepting electrons with a low energetic cost, so that such bands be partially occupied. Therefore, depending on the distribution of the molecules within the material and on the extent of the electronic transfer, different band structures are formed and, consequently, compounds that may be insulating, semiconducting, metallic or superconducting may be obtained. For many years, most research had dealt with inorganic materials, until the potential of the organic and metalorganic derivatives became clear when it was reported that the tetrathiofulvalene chloride was electrically conducting at the relatively low temperatures between 50 and 60 K [6,7], and the application of (organo-) aluminum compounds as thin films for microelectronics was reported [8]. In the following years, a lot of effort has been oriented to the formation and characterization of molecular-material thin films as an important step towards their use in organic-based devices [9–12]. On the other hand, research on molecular electronics involving transition metal complexes has received an increasing interest based on the fact that the oxidation states of transition metals can be varied to a great extent and thus that many electron transfer processes can result [6,7,13]. Several studies of materials containing metallic complexes have been reported to date [13–18]. Some important examples are the first superconductor with a paramagnetic metal ion, $(BEDT–TTF)_4A[Fe(C_2O_4)_3]$ (BEDT–TTF = bis(ethylenedithio)tetrathiafulvalene and A = K, NH_4, H_2O) [17]; the first molecular metallic ferromagnet $(BEDT–TTF)_3[Mn^{II}Cr^{III}(C_2O_4)_3]$, which was formed by infinite sheets of the magnetic coordination polymer interleaved with layers of conducting BEDT–TTF cations, and shows ferromagnetism and metallic conductivity [18]. Hybrid compounds based on dimetallic $M^{II}M^{III}$ oxalate complexes (M^{III} = Cr, Fe; M^{II} = Mn, Fe, Co, Ni, Cu and Zn) and TTF molecules have also been reported

* Corresponding author.
E-mail address: elena.sanchez@anahuac.mx (M.E. Sánchez-Vergara).

0169-4332/$ – see front matter © 2010 Elsevier B.V. All rights reserved.
doi:10.1016/j.apsusc.2010.11.011

[19], as well as thin films obtained from $[TiO(C_2O_4)_2]^{2-}$ anionic complexes and n-octadecylamine [20].

In view of the fact that metal oxalate complexes have demonstrated to be promising building blocks to obtain multilayered molecular-based materials, the purpose of this work is to explore $A_2[TiO(C_2O_4)_2]$ (A = K, PPh_4) and 1,8 dihydroxyanthraquinone ($C_{14}H_8O_4$) and its potassium salt ($K_2C_{14}H_6O_4$) as building blocks to synthesize molecular material thin films. Thermal evaporation and ellipsometry have been employed in the growth and characterization of the thin films, respectively. The refractive indices and absorption coefficients have been determined for the studied samples, since both parameters are of particular interest in the design and fabrication of optoelectronic devices [21,22]. The optical band gap and electrical properties, such as the electrical conductivity and activation energy of the resulting thin films, have also been measured. The third harmonic generation (THG) technique was chosen to measure the $\chi^{(3)}$ values because it allows the measurement of pure electronic NLO-effects, which are important for semiconducting and photonic applications.

2. Experimental procedure

The raw materials for this work were obtained from commercial sources and used with no further purification. $(PPh_4)_2[TiO(C_2O_4)_2]$ was obtained from the reaction of $K_2[TiO(C_2O_4)_2]$ with $(PPh_4)Cl$ in water. Cyclical-voltammetry experiments were carried out for the starting material with an Autolab PGSTAT30 system in a conventional three-electrode mode. FT-IR spectra were acquired with a PerkinElmer IR spectrophotometer model 282-B using KBr pellets. Fast atomic bombardment (FAB+) mass spectroscopy of the powder samples was performed on a 3-nitrobenzyl alcohol support in the positive ion mode on a *Jeol* spectrometer, model *JMS-SX102A*.

For the thin films, FT-IR measurements were obtained with a spectrophotometer Nicolet 5-MX. AFM (atomic force microscopy) images were obtained using a Jeol JSPM-4210 in contact mode, tapping and NSCIS (non-contact silicon cantilevers). Ellipsometric measurements were made using a Gaertner Model L117 ellipsometer with a He–Ne laser operating at 630 nm. UV–vis absorbance measurements were made with a Shimadzu 260 double-beam spectrophotometer. A four-probe press contact method was employed to measure the electrical conductivity of the sample within a working temperature range between 295 and 450 K. Silver paint was applied to the sample to form an ohmic contact and the temperature dependence of the electrical conductivity was measured with a Keithley 230 programmable voltage source and a Keithley 485 auto-ranging pico-ammeter, both PC-controlled. The temperature of the sample was measured with a chromel–alumel thermocouple attached to an HP 3421 data acquisition unit.

2.1. Synthesis

An ethanolic solution of $A_2[TiO(C_2O_4)_2]\cdot nH_2O$ (A = K, PPh_4) was added either to 1,8 dihydroxyanthraquinone ($C_{14}H_8O_4$) or to its postasium salt ($K_2C_{14}H_6O_4$) also dissolved in ethanol. The mixtures were refluxing for 72 h. The obtained solids were filtered off, washed with absolute ethanol and vacuum dried. The four new products were recrystallized in a 1:1 ethanol-water solution giving materials **A** to **D**.

Material **A:** 0.8 g (0.87 mmol) of $(PPh_4)_2[TiO(C_2O_4)_2]$, 0.4 g (1.74 mmol) of $C_{14}H_8O_4$. Yield reaction 93%. M.p. 306 °C (dec). MS(FAB^+, DMSO/EtOH) *m/z*: 305 $[TiO(C_{14}H_8O_4)]^+$, 241 $[C_{14}H_8O_4]^+$, 339 $[PPh_4]^+$, 77 $[Ph]^+$.

Material **B:** 0.4 g (1.26 mmol) of $K_2[TiO(C_2O_4)_2]$, 0.6 g (2.54 mmol) of $C_{14}H_8O_4$. Yield reaction 89%. M.p. 311 °C (dec). MS(FAB^+, DMSO/EtOH) *m/z*: 391 $[TiO(C_2O_4)(C_{14}H_8O_4)]^+$, 305 $[TiO(C_{14}H_8O_4)]^+$, 241 $[C_{14}H_8O_4]^+$, 39 $[K]^+$.

Material **C:** 0.3 g (0.33 mmol) $(PPh_4)_2[TiO(C_2O_4)_2]$, 0.2 g (0.66 mmol) of $K_2C_{14}H_6O_4$. Yield reaction 86%. M.p. 298 °C (dec). MS(FAB^+, DMSO/EtOH) *m/z*: 305 $[TiO(C_{14}H_8O_4)]^+$, 241 $[C_{14}H_8O_4]^+$, 339 $[PPh_4]^+$, 77 $[Ph]^+$.

Material **D:** 0.3 g (0.94 mmol) $K_2[TiO(C_2O_4)_2]$, 0.6 g (1.88 mmol) of $K_2C_{14}H_6O_4$. Yield reaction 88%. M.p. 309 °C (dec). MS(FAB^+, DMSO/EtOH) *m/z*: 391 $[TiO(C_2O_4)(C_{14}H_8O_4)]^+$, 305 $[TiO(C_{14}H_8O_4)]^+$, 241 $[C_{14}H_8O_4]^+$, 39 $[K]^+$.

2.2. Thin films preparation

Thin-film deposition was carried out onto 7059 Corning glass slices and (1 0 0) single-crystalline silicon (c-Si) wafers. The Corning glass substrates were ultrasonically degreased in warm methanol and dried within a nitrogen atmosphere. The silicon wafers underwent chemical etching with a *p* solution (10 ml HF, 15 ml HNO_3 and 300 ml H_2O) in order to remove the native oxide from the surfaces. To prevent powder products from accumulating on the substrate surface, the evaporation source was a molybdenum boat with two grids. The evaporation temperature in the boat was lower than the decomposition temperature of the synthesized materials, about 280 °C. All samples were obtained using the same deposition system, with the crucible and substrates disposed in the same geometry. The base pressure (10^{-1} Torr) in the chamber before thin film deposition and the amount of mass inside the crucible were the same in all cases. For infrared, AFM and ellipsometric measurements, the substrates were oriented along the (1 0 0) direction. Each substrate was made of 200 (S cm) c-Si. For the optical transmission measurements, the substrates were bare 7059 Corning glass slices. The electrical conductivity of the films was studied by means of a four-probe using 7059 Corning glass substrates coated with four metallic strips. These metallic strips acted as electrodes for the electrical measurements. In order to get an ohmic behavior between the deposited films and the metallic electrodes, four chromium strips were deposited by vacuum thermal evaporation onto the glass slices. Finally, measurements of the cubic NLO-properties according to the THG-Maker fringes technique were performed in the glass-substrate coated samples. The experimental setup basically consisted of a Q-switched Nd:YAG laser system (Surelite II from Continuum, λ_ω = 1064 nm, repetition rate of 10 Hz and a pulse width of $\tau \approx 22$ ns), which provided the fundamental wave. Typical pulse powers of 80 μJ were filtered in order to irradiate the samples by means of an *f* = 50 mm focusing lens, thus peak irradiances on the order of 1.8 GW cm^{-2} were achieved at the focal spot on the film samples. This value was slightly below the damage threshold energy supported by the samples under strong focused beam irradiation. The polarization of the fundamental beam (S or P polarizing geometry) was selected by means of an IR-coated Glan-Laser polarizer and a λ/2-quartz-retarder. A second polarizer, used as an analyzer, allowed the characterization of the THG-response. The third harmonic wave ($\lambda_{3\omega}$ = 355 nm) was detected by a sensitive photomultiplier tube placed behind interference optical filters centered at 355 nm. The THG-device was previously calibrated by means of a fused silica plate ($\chi^{(3)} \approx 3.11 \times 10^{-14}$ esu, at λ_ω = 1064 nm), which is frequently used as a NLO-reference standard via the Maker fringes method. The THG measurements were performed for incident angles in the range from −45° to +45°.

3. Results and discussion

Starting-material cyclic voltamperograms were recorder in an ethanolic solution using $LiClO_4$ (1 M) as support electrolyte and a cell with a calomel reference electrode and platinum electrodes

Please cite this article in press as: E. Carbia-Ruelas, et al., Electrical and optical properties of thermally-evaporated thin films from $A_2[TiO(C_2O_4)_2]$ (A = K, PPh_4) and 1,8-dihydroxyanthraquinone, Appl. Surf. Sci. (2010), doi:10.1016/j.apsusc.2010.11.011

Table 1
IR characteristic bands for powder and thin films (cm^{-1}).

Compound	νarm(C–H)	ν(COO)	νarm(C–C)	ν(C–O)	δ(OCO)
A (powder)	3041	1674	1625	1271	778
A (thin film)	3043	1674	1625	1273	779
B (powder)	3069	1720, 1684	1625	1269	783
B (thin film)	3070	1720, 1685	1624	1269	785
C (powder)	3063	1671	1624	1266	746
C (thin film)	3062	1670	1624	1265	744
D (powder)	3044	1720, 1686	1611	1263	753
D (thin film)	3047	1720, 1686	1612	1265	750

operating as the working electrode and as counter-electrodes, respectively. They show ΔE_{redox} in the range of 0.05–0.9 V for the redox potential between the acceptor and donor, with an oxidation potential of at least 1.7 V for the organic compound and a reduction potential of 1.75 V for the titanium complex. These values are in the range established by Saito and Ferraris for promising organic metal materials ($-0.02 \leq \Delta E_{redox} \leq 0.34$ V) [4].

FT-IR spectroscopy was performed on both powder samples and thin films to determine the presence of the representative bond vibration modes of the synthesized compounds and to determine if there were significant chemical changes in these materials during the thermal evaporation process. The presence of new aromatic ν(C–H) and ν(C–C) signals around 3070–3040 and 1625–1605 cm^{-1} in powder samples (**B** and **C**) indicate the attachment of the donor. The ν(C=O) and ν(C–O) bands were found in the range of 1720–1660 and around 1270 cm^{-1}, respectively. The values for the characteristic IR bands of the thin films are very close to those observed for the original powder compounds on potassium bromide (KBr) pills (Table 1); this suggests that there was not decomposition during the process of getting the thin films, so they kept their initial chemical structure. The slight modifications observed in these values may be due to internal stress produced by the evaporation process.

Despite the relatively low solubility of the obtained powder compounds, the positive-ion FAB mass spectra have shown signals for $[C_{14}H_8O_4]^+$ (241 *m/z*) and fragments containing titanium, $[TiO(C_{14}H_8O_4)]^+$ (305 *m/z*), $[TiO(C_2O_4)(C_{14}H_8O_4)]^+$ (391 m/z), confirming the presence of the donor. Signals were also found for $[K]^+$ (39 *m/z*) in **B**–**D** spectra, and for $[Ph]^+$ (77 *m/z*) and $[PPh_4]^+$ (339 *m/z*) in **A** and **C** spectra. All of the observed signals exhibit the expected characteristic isotropic distribution patterns. Two approaches might explain the acceptor-donor interaction in these new synthesized materials. First, the inclusion of the donor into the coordination sphere of titanium might occur, $[TiO(C_2O_4)_2(C_{14}H_6O_4)]^{-n}$, as it was proposed in the complex between titanyl oxalate and 3-hydroxyflavone, $[TiO(C_2O_4)_2(C_{15}H_9O_3)_2]^{-4}$ [23]. On the other hand, it is also possible that a multilayer metallic charge-transfer salt was formed with an arrangement somehow similar to that of $(BEDT\text{–}TTF)_4A[Fe(C_2O_4)_3]$ (A = K, NH_4, H_2O), in which successive layers of BEDT–TTF and layers containing alternating **A** and $Fe(C_2O_4)_3^{-3}$ was observed [17], $(C_{14}H_6O_4)_xA_y[TiO(C_2O_4)_2]\cdot nH_2O$ (A = K, PPh4).

The morphology and roughness of the thin films were examined by atomic force microscopy in order to provide a large surface inspection of the micro-structural arrays, topological structure, porosity and film quality of the deposited layers as summarized in Fig. 1, where 3D micrographs are shown, and Table 2. For thin-film samples made from materials **A** and **C**, one can observe small-particle agglomeration, a homogeneous distribution and some spots on the surface (Fig. 1A and C). In the case of films **B** and **D** as obtained from $K_2[TiO(C_2O_4)_2]$, small particles agglomerate to generate huge rounded grains, showing still a reasonably homogeneous distribution at large micrometric length scales (see Fig. 1B and D). These latter arrangements show the largest roughness with small inter-grain porosity (Table 2). It is worth noting that the largest rugosity is shown by films synthesized from the potassium double salt of 1,8-dihydroxyanthraquinone (materials **C** and **D**). It is important to point out that the morpho-

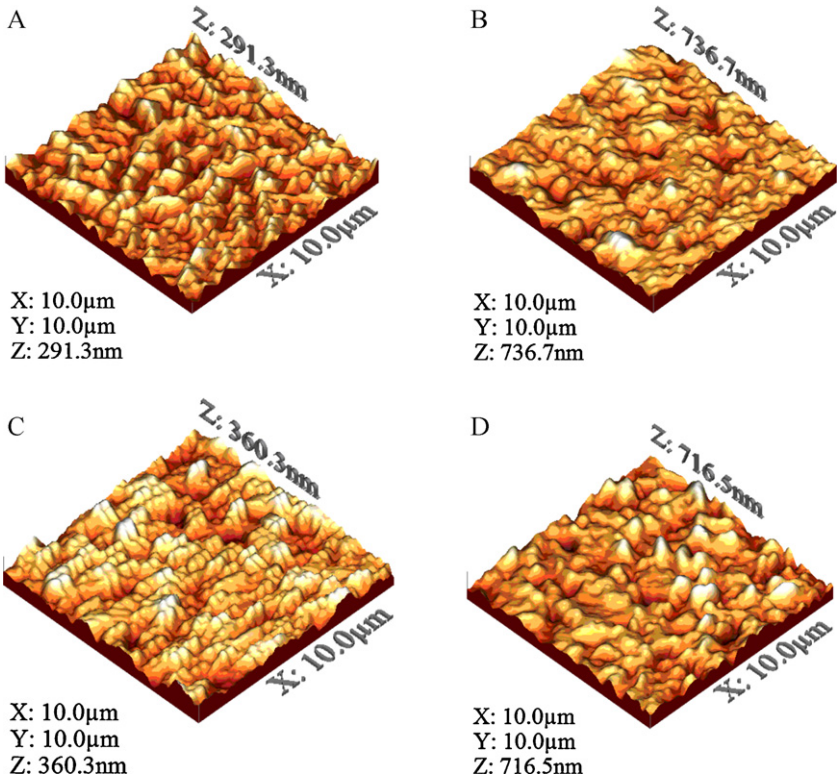

Fig. 1. 3D-micrographs obtained by AFM showing the surface morphology of thin films **A**, **B**, **C** and **D**.

Please cite this article in press as: E. Carbia-Ruelas, et al., Electrical and optical properties of thermally-evaporated thin films from $A_2[TiO(C_2O_4)_2]$ (A = K, PPh_4) and 1,8-dihydroxyanthraquinone, Appl. Surf. Sci. (2010), doi:10.1016/j.apsusc.2010.11.011

Table 2
Characteristic parameters of investigated thin-film.[a]

Sample	RMS (AFM) (nm)[b]	Refractive index, n	Reflectance, R (%)	d (nm) [c]	Eg_i (eV)[d]	Eg_d (eV)[e]	σ ($S^{-1}cm^{-1}$)[f]	E_a (eV)[g]
A	32.7	2.16	13.53	306	1.7	2.15	0.5×10^{-5}	0.03 0.003
B	60.1	2.26	14.94	305	1.6	1.90	0.75×10^{-5}	0.040
C	43.0	2.17	13.62	372	1.7	2.00	0.63×10^{-5}	0.015 0.008
D	74.9	2.19	13.86	278	2.0	2.30	0.8×10^{-5}	1.16

[a] d: film thickness; Ea: activation energy; Eg_d and Eg_i: direct and indirect band gap, respectively; σ: electrical conductivity at 25 °C.
[b] ±1.5% tolerance.
[c] ±5% tolerance.
[d] ±15% tolerance.
[e] ±15% tolerance.
[f] ±10% tolerance.
[g] ±10% tolerance.

logical variations observed in the film samples will affect important physical properties, such as the optical properties of the materials.

Taking into account the thermal decomposition temperatures, the electrical conductivities of the materials were measured in the 295–450 K temperature range. By analyzing the shape of $\ln\sigma = f(1000/T)$ graphs in Fig. 2, useful information regarding the processes occurring in the investigated thin films during the heat treatment can be obtained. The dc conductivity has the general form,

$$\sigma = \sigma_0 \exp\left(-\frac{E_a}{kT}\right) \quad (1)$$

where E_a is the thermal activation energy of the electrical conductivity, σ_0 is the pre-exponential factor depending on the material's nature, and k is Boltzmann's constant. A plot of $\ln\sigma$ versus $1000/T$ yields a straight line whose slope can be used to determine the thermal activation energies of the thin films [24]. Calculated values of E_a are shown in Table 2, as well as the electrical conductivity σ at 25 °C for all studied materials. These σ values are very similar and lie within the semiconductor region (10^{-6} to 10^{2} S/cm) [25]. In ordinary semiconductors, conductivity is also related to impurity types, their location and concentration, crystal structure, stacking and orbital overlap. Holes in the valence band and electrons in the conduction band contribute to the electrical conductivity. Multiple donor levels exist within the forbidden energy gap and the deeper levels can be frozen out as the temperature is increased [14–16].

Generally speaking, electric conductivity changes little within this group of materials. By analyzing Fig. 2, the curves for the materials **A** and **C** are characterized by two sections with different slopes. The calculated activation energies are related to different processes concerning these sections. The lower values of E_a are associated with the intermolecular conduction processes, while the higher values are related to the intramolecular conduction processes [24]. In these semiconducting materials, there are two stages describing the movement of carriers within the sample. In the intramolecular transfer of electrons, electrons can hop from one atomic site to another if orbitals exist at these sites with the same energy levels. In the case of intermolecular orbital overlap, electrons or holes can travel from one kind of molecule, i.e., $A_2[TiO(C_2O_4)_2]$, to another. Therefore, π-electrons can also hop from one type of molecule to another if orbitals with the same energy levels exist between the complex molecules. If we assume excited carriers within the molecules, the carriers are retarded by the barrier molecules. The activation energy of the intramolecular conduction process is then higher. Therefore, the primary site for conduction must be found between molecules since the lower activation energy corresponds to intermolecular transfer, while the higher activation energy corresponds to intramolecular transfer. In any case, both processes should be considered. The intramolecular conduction process occurs between the metal atom and the ligands in the complex and the intermolecular conduction process occurs between two molecule complexes [24].

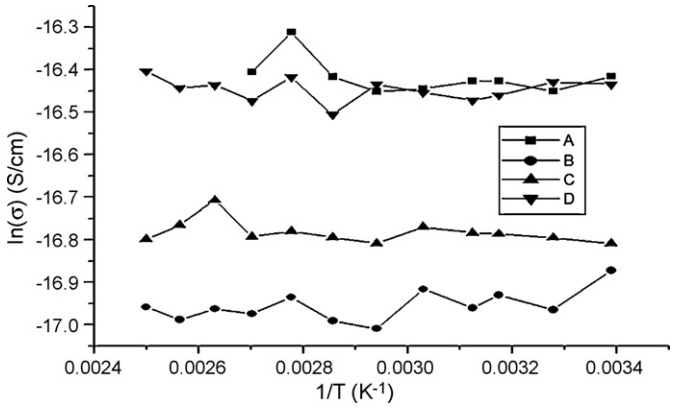

Fig. 2. Temperature dependence of the electrical conductivity for **A**, **B**, **C** and **D** thin films.

The electrical conductivities of the materials **A** and **C** have positive temperature coefficients. That is, conductivity increases exponentially with temperature. The increase starts as soon as charge carriers acquire large enough activation energies. The mobility of these carriers also increases with temperature. This is a property of typical semiconductors. Nevertheless, the electrical conductivities of the compounds have negative heat coefficients above 350–380 K,. Measurements showed that these complexes have n-type electrical conductivity, that is, most of the carriers are electrons [24]. Materials **B** and **C** show a rather weak semiconducting behavior in the range of temperatures used for these measurements.

The thickness, refractive index and reflectance of each layer were determined by ellipsometry. Some differences in the thickness of the deposited films were detected which may be related to differences in the evaporation processes for the compounds used. The thickness varies from 278 to 372 nm (Table 2); hence, the Beer–Lambert law applies for such semi-transparent thin-film systems. The absorption coefficient (α) is defined by the Beer–Lambert law and can be calculated from the optical transmittance [26].

$$\alpha = -\ln(T/t) \quad (2)$$

where T is the transmittance and is related to the absorbance A according to $A = -\log(T)$; t is the film thickness. The optical absorption of the studied compounds and the precursor thin films deposited on Corning 7059 glass slices were studied in the wavelength range 190–1090 nm. Fig. 3 shows the graph of transmittance versus wavelength (λ) for the A–D films. The band around 440 nm is due to electronic transitions between molecules having an intermediate ionic degree that conform the synthesized molecular materials. In order to evaluate the nature of the transition (direct

Please cite this article in press as: E. Carbia-Ruelas, et al., Electrical and optical properties of thermally-evaporated thin films from $A_2[TiO(C_2O_4)_2]$ (A = K, PPh_4) and 1,8-dihydroxyanthraquinone, Appl. Surf. Sci. (2010), doi:10.1016/j.apsusc.2010.11.011

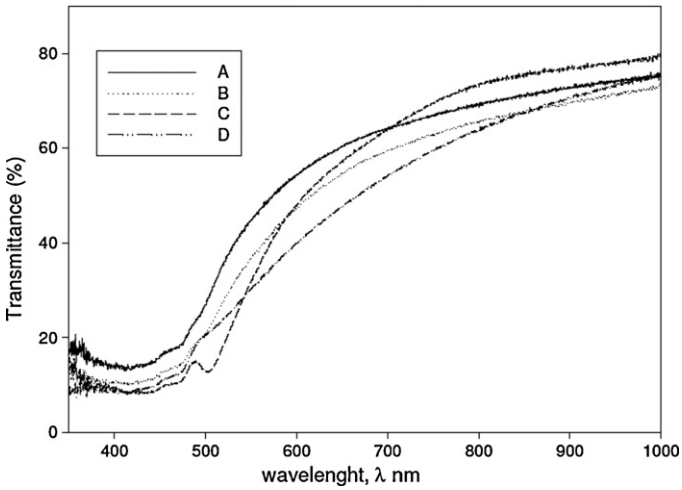

Fig. 3. Transmittance vs. wavelength for materials **A**, **B**, **C** and **D**.

or indirect), the relation [27]:

$$\alpha h\upsilon = A(h\upsilon - E_g)^n \quad (3)$$

deduced for the domain of fundamental absorption edge, was used. In this relation, α denotes the absorption coefficient, $h\upsilon$ the photon energy, E_g the band gap energy, n a number characterizing the transition process and A is a characteristic parameter for the corresponding transitions and can be assumed to be constant within the optical frequency range [28]. For allowed direct transitions, $n = ½$, and for allowed indirect transitions $n = 2$. Thus, the optical gaps for both transitions could be determined by the extrapolation to zero of the linear regions of the $(\alpha h\upsilon)^2 = f(h\upsilon)$ and $(\alpha h\upsilon)^{1/2} = f(h\upsilon)$ curves, Eg_d and Eg_i, respectively (Table 2) [29].

The straight line nature of the plots over a wide range of photon energy indicates direct and indirect types of transition. Fig. 4 exhibits a representative example of the typical absorption curves of one of the investigated samples that shows evidence for both direct and indirect transitions. In amorphous semiconductors, the optical transitions are dominated, to a first approximation, by the so-called indirect transitions. In these electronic transitions from states in the valence band to states in the conduction band, there is no conservation of the electronic momentum [30]. However, as can be seen in Fig. 4 and for all the materials, direct transitions (E_{gd}) are related to a more linear behavior for the referred curves. For the direct transition, the squared absorption coefficient is a linear function of the incident photon's energy (Fig. 4), which is related to the one-electron theory of Bardeen et al. [31,32]. This theory has been successfully applied to analyze the absorption edge of different amorphous semiconductors. The absorption ($\alpha > 10^4\ cm^{-1}$) is related to direct interband transitions where the lowest part of the valence band and the highest part in the conduction band share the same wave vector and there is an allowed transition across the band gap.

Table 3
$\chi^{(2)}$ values for the derived molecular films.

Sample	$\chi^{(3)}$ values $\times 10^{-14}$ (esu)
Reference: Fused silica	3.11
Material **A**	47.2
Material **B**	71.7
Material **C**	55.3
Material **D**	86.4

Finally, according to the amorphous nature of the synthesized compounds (verified by the absence of quadratic $\chi^{(2)}$ -NLO second harmonic generation effects), the cubic $\chi^{(3)}$ -NLO properties were investigated by means of the optical THG-technique in the developed solid-state film structures at room conditions. Experimental single-beam techniques based on THG give direct access to the complex value of the non-degenerate $\chi^{(3)}(-3\omega, \omega, \omega, \omega)$ cubic nonlinear coefficient; the advantage here is the fact that the THG-response accounts only for the electronic response, so that vibrational, orientational, and thermal effects, which may contribute to the overall non-linear response of the material, are excluded. Table 3 shows the calibrated nonlinear optical $\chi^{(3)}$ -coefficients of the studied thin film samples according to the Maker fringes. In Fig. 5, we report typical Maker fringe patterns (front-configuration, P/In-P/Out polarizing geometry and resonant configuration at $\lambda_\omega = 1064$ nm and $\lambda_{3\omega} = 355$ nm) of the studied thin films; these data are compared to the fringe pattern generated by the 1 mm thick substrate alone. The Maker fringe patterns of the molecular film-plus-substrate systems show a similar oscillating dependence with increasing incident angles compared to the fringes measured for the reference substrate. This indicates that the glass substrate dominates the NLO-process due to the small thickness of the films. Nevertheless, these fringes are clearly more intense than those recorded for the substrate alone, which indicates relatively stronger THG-conversion of the studied molecular films. The lack of sharp multi-oscillations in some measurements is due to the fact that the thickness of the studied films was shorter than their characteristic coherence lengths (usually in the range of a few microns); thus, the THG-intensity would not follow the phase-matching oscillations that depended on the medium thickness. Furthermore, the strong absorption conditions experienced with the available excitation wavelength and the scattering effects observed for the **B** and **D** samples partially overshadow the

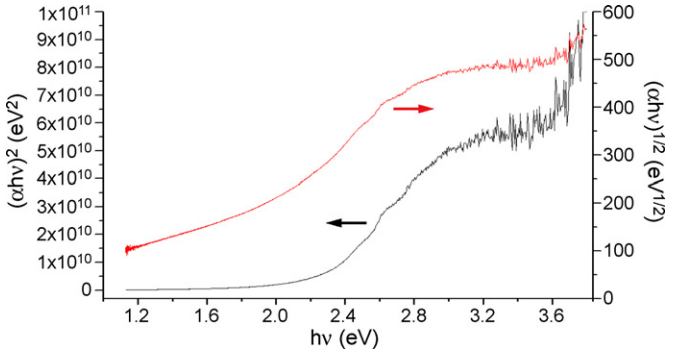

Fig. 4. Absorption curves (material **B**) illustrating direct (curve 1) and indirect (curve 2) gap.

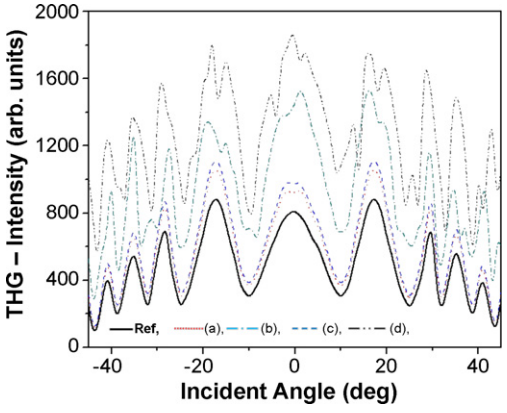

Fig. 5. THG-nonlinear optical Maker-fringe measurements for the reference substrate and: (a) **A**-, (b) **B**-, (c) **C**- and (d) **D**-based thin films, respectively.

Please cite this article in press as: E. Carbia-Ruelas, et al., Electrical and optical properties of thermally-evaporated thin films from $A_2[TiO(C_2O_4)_2]$ (A = K, PPh_4) and 1,8-dihydroxyanthraquinone, Appl. Surf. Sci. (2010), doi:10.1016/j.apsusc.2010.11.011

Maker fringe oscillations. Indeed, the THG-response obtained at nearly normal incidence gives the highest conversion efficiency, which permits the relative evaluation of the $\chi^{(3)}$ -coefficients. As a first estimation of the cubic NLO-properties of these materials, and considering samples under resonant (absorption) conditions, the determination of $\chi^{(3)}$ may be approximated by the following expression [33]:

$$\chi^{(3)-\text{Film}} \equiv \chi^{(3)-\text{Reference}} \left(\frac{2l_c^{\text{Reference}}}{\pi}\right)\left(\frac{\alpha/2}{1-e^{-\alpha l_{\text{Film}}/2}}\right)\left(\frac{I_{3\omega}^{\text{Film}}}{I_{3\omega}^{\text{Reference}}}\right)^{1/2} \quad (4)$$

where α is the absorption coefficient of the film sample at the third harmonic free-wave and $l_c^{\text{Reference}}$ represents the coherence length of the reference material (~8 μm). $\chi^{(3)-\text{Film}}$ and $\chi^{(3)-\text{Reference}}$ are, respectively, the values of the cubic nonlinear coefficients of the film samples and the fused silica plate, while $I_{3\omega}^{\text{Film}}$ and $I_{3\omega}^{\text{Reference}}$ are the peak intensities of the Maker fringe patterns of the film sample and the reference plate, respectively. In this way, the $\chi^{(3)}$ value of a new material relative to the value of the reference standard can be obtained; hence, a calibrated result with a high degree of accuracy can be reported.

In principle, both the film and the substrate contribute to the detected THG-signal (the focal length of the focusing lens is less than 50 mm in order to make the air contribution to the THG-signal negligible; these two contributions must be separately identified in order to give a good estimate of the $\chi^{(3)-\text{Film}}$ coefficients). Moreover, since the film is deposited only on one side of the substrate, the experimental configuration is asymmetric from a geometrical viewpoint and different relations have been developed in order to fit respectively the 'front' configuration where the fundamental beam enters the film, or the 'back' configuration, where the films stay behind the substrate [34–40]. Under this framework, Table 3 shows the $\chi^{(3)-\text{Film}}$ calibrated coefficients according to Equation 3 and Fig. 5 (front configuration). The highest cubic NLO-coefficient was evaluated for the **D-**based thin-film sample, followed by the **B-**, **C-** and **A-**based thin films, respectively. A substantial decrease of the $\chi^{(3)-\text{Film}}$ value occurs for the samples not containing a potassium atom in the final product.

It could be verified that the diverse molecular systems produced notable differences in their linear and nonlinear optical properties. Particularly, the cubic NLO effects were considerably improved in films of materials synthesized from $K_2[TiO(C_2O_4)_2]$, i.e. **B** and **D**. These samples exhibited higher conjugation degrees and conductivities, lower optical absorption and band-gap values, and apparently adequate electronic multi-level organizations, which were sensitively detected and verified by NLO-THG measurements. In addition to the distinctive differences provoked by the diverse chemical structures and their corresponding physical properties on the THG-responses, another correlation attributed to the thin film structures (variations on the rugosity, see Table 2) could also be established. Despite the observed differences in the film thicknesses, the film structures may also play an important role regarding the origin and magnitude of the observed THG-signals, as it is observed that the most THG-efficient **D-** and **B-**based film samples also show the highest rugosity. In the specific case of compound **D**, its higher conductivity and the delocalization of its conjugated electronic system assures the largest cubic NLO phenomena.

4. Conclusions

Molecular materials from $A_2[TiO(C_2O_4)_2]$ (A = K, PPh_4) and 1,8-dihydroxyanthraquinone were synthesized. Their thin films were deposited by vacuum thermal evaporation. According to the IR spectra, they are formed by the same chemical units as those of the corresponding synthesized powders. Thus, the thermal evaporation process can be, in general, considered as a molecular process. The substrate temperature is not high enough to provide the necessary surface mobility for the molecular units to produce highly ordered crystalline films. On the other hand, the AFM analysis shows that deposition of thin films over the layers occurs despite some rugosity and that the film depositions were quite uniform and homogeneous, providing trustworthy electrical and optical characterization tests. The thin films of the synthesized molecular materials show electrical conductivities at room temperature of the order of 10^{-5} (S cm), which suggests a semiconducting behavior. The electron transport in the investigated compounds is strongly influenced by their molecular structures. Thin films produced from **D** and **B** compounds exhibited a larger conductivity which, in combination with a higher degree of conjugation of the delocalized π-electron system, allowed the most favorable conditions to generate efficient cubic NLO-effects such as THG. The measurement of cubic-only, non-degenerated χ (3) (-3ω; ω, ω, ω) NLO coefficients in all the studied samples, instead of quadratic- χ (2) ones, pointed out to predominantly amorphous structured-molecular arrangements. The cubic NLO effects were substantially enhanced for materials synthesized from $K_2[TiO(C_2O_4)_2]$ (**B** and **D**) where $\chi^{(3)}$ (-3ω; ω, ω, ω) values in the promising range of 10^{-12} esu have been evaluated.

Acknowledgments

Financial support from SEP-CONACyT (grant: 82808-J2 and 102401) is gratefully acknowledged. The authors acknowledge the technical assistance of Carlos Flores Morales, José Chavez Carvayar and Arturo Rodriguez Gomez (IIM-UNAM).

References

[1] F. Wudl, Acc. Chem. Res. 17 (1984) 227.
[2] J.R. Ferrraro, J.M. Williams, Introduction to Synthetic Electrical Conductors, Academic Press, London, 1987.
[3] M.R. Bryce, J. Mater. Chem. 10 (2000) 589.
[4] G. Saito, J.P. Ferraris, Bull. Chem. Soc. Jpn. 26 (1980) 2141.
[5] D. Astruc, Acc. Chem. Res. 30 (1997) 383.
[6] F. Wudl, D. Wobschall, E.J. Hufnagel, J. Am. Chem. Soc. 94 (1972) 671.
[7] J. Ferraris, D.O. Cowan, V. Walatka, J.H. Perlstein, J. Am. Chem. Soc. 95 (1973) 948.
[8] G.B. Stringfellow, Organometallics Chemical Vapor Epitaxy: Theory and Practice, Academic Press, New York, 1989.
[9] R.A. Laudise, C. Kloc, P.G. Simpkins, T. Siegrist, J. Cryst. Growth 187 (1998) 449.
[10] J. Caro, S. Garelik, A. Figeras, Chem. Vap. Deposition 2 (1996) 251.
[11] A. Figueras, S. Garelik, J. Caro, J. Cifré, J. Veciana, C. Rovira, E. Ribera, E. Canadell, A. Seffar, J. Fontcuberta, J. Cryst. Growth 166 (1996) 798.
[12] S. Molas, J. Caro, J. Santiso, A. Figueras, J. Fraxedas, C. Méziere, M. Fourmigue, P. Batail, J. Cryst. Growth 218 (2000) 399.
[13] H.E. Toma, J. Braz. Chem. Soc. 14 (2003) 845.
[14] P. Cassoux, D. De Caro, L. Valade, H. Casellas, B. Daffos, M.E. Sánchez Vergara, Mol. Cryst. Liq. Cryst. Sci. Technol. Sect. A 380 (2002) 45.
[15] M.E. Sánchez-Vergara, A. Ortiz-Rebollo, J.R. Álvarez, M. Rivera, J. Phys. Chem. Solids 69 (2008) 1.
[16] A. Rodríguez, M.E. Sánchez-Vergara, V. García-Montalvo, A. Ortiz, J.R. Alvarez, Appl. Surf. Sci. 256 (2010) 3374.
[17] M. Kurmoo, A.W. Graham, P. Day, S.J. Coles, M.B. Hurtshouse, J.L. Caulfield, J. Singleton, F.L. Pratt, W. Hayes, L. Ducasse, P. Guionneau, J. Am. Chem. Soc. 117 (1995) 12209.
[18] E. Coronado, J.R. Galán-Mascarós, C.J. Gómez-García, V. Laukhin, Nature 408 (2000) 447.
[19] E. Coronado, J.R. Galán-Mascarós, C. Giménez-Saiz, C.J. Gómez-García, C. Ruiz-Pérez, Eur. J. Inorg. Chem. (2003) 2290.
[20] P. Ganguly, D.V. Paranjape, M. Sastry, Langmuir 9 (1993) 577.
[21] M. Sridharan, S.K. Narayandass, D. Mangalaraj, J. Mater. Sci.: Mater. Electr. 13 (2002) 471.
[22] P.N. Prasad, D.J. Williams, Introduction to Nonlinear Optical Effects in Molecules and Polymers, Wiley Interscience, New York, 1991 (Chapter 1).
[23] M. Aleksic, S. Blagojevic, D. Malesec, Z. Radovic, J. Serb. Chem. Soc. 65 (2000) 631.
[24] S. Sarkar, Y. Aydogdu, F. Dagdelen, B.B. Bhaumik, K. Dey, Mater. Chem. Phys. 88 (2004) 357.
[25] M.S. Kiani, G. RMitchell, Synth. Met. 46 (1992) 293.
[26] X. Li, H. Zhu, J. Wei, K. Wang, E. Xu, Z. Li, D. Wu, Appl. Phys. A 97 (2009) 341.

Please cite this article in press as: E. Carbia-Ruelas, et al., Electrical and optical properties of thermally-evaporated thin films from $A_2[TiO(C_2O_4)_2]$ (A = K, PPh_4) and 1,8-dihydroxyanthraquinone, Appl. Surf. Sci. (2010), doi:10.1016/j.apsusc.2010.11.011

[27] L. Leontie, M. Caraman, M. Delibas, G.I. Rusu, Mater. Res. Bull. 36 (2001) 1629.
[28] M.M. El-Nahass, A.M. Farag, K.F. Abd El-Rahman, A A.A. Darwish, Dispersion studies and electronic transitions in nickel phthalocyanine thin films, Opt. Laser Technol. 37 (2005) 513.
[29] L. Leontie, M. Roman, F. Brinza, C. Podaru, G.I. Rusu, Synth. Met. 138 (2003) 157.
[30] CodyF G.D., in: J.I. Pankove (Ed.), Hydrogenated Amorphous Silicon, Part B, Optical Properties, Semiconductors and Semimetals, vol. 21, Academic Press, Orlando, 1984.
[31] M.M. El-Nahass, K.F. Abd-El-Rahman, A.A. Al-Ghamdi, A.M. Asiri, Physica B 344 (2004) 398.
[32] J. Bardeen, F.J. Slatt, L.J. Hall, Photoconductivity Conference, Wiley, New York, 1956, p. 146.
[33] F. D'Amore, A. Zappettini, G. Facchini, S.M. Pietralunga, M. Martinelli, C. Dell'Erba, C. Cuniberti, D. Comoretto, G. Delle Piane, Synth. Met. 127 (2002) 143.
[34] F. D'Amore, M. Di Giulio, S.M. Pietralunga, A. Zappettini, L. Nasi, V. Rigato, M. Martinelli, J. Appl. Phys. 94 (2003) 1654.
[35] H. Nakanishi, H. Matsuda, S. Okada, M. Kato, Polym. Adv. Technol. 1 (1990)75.
[36] B. Buchalter, G.R. Meredith, Meredith Appl. Opt. 21 (1982) 3221.
[37] G.R. Meredith, Phys. Rev. B 24 (1981) 5522.
[38] X.H. Wang, D.P. West, N.B. McKoewn, T.A. King, J. Opt. Soc. Am. B 15 (1998) 1895.
[39] K. Miyano, T. Nishiwaki, A. Tomioka, Opt. Commun. 91 (1992) 501.
[40] D.S. Bethune, J. Opt. Soc. Am. B 6 (1989) 910.

Please cite this article in press as: E. Carbia-Ruelas, et al., Electrical and optical properties of thermally-evaporated thin films from $A_2[TiO(C_2O_4)_2]$ (A = K, PPh_4) and 1,8-dihydroxyanthraquinone, Appl. Surf. Sci. (2010), doi:10.1016/j.apsusc.2010.11.011